🔵 **PLOS** | ONE

# A Conserved Rule for Pancreatic Islet Organization

**Danh-Tai Hoang[1], Hitomi Matsunari[2], Masaki Nagaya[2], Hiroshi Nagashima[2], J. Michael Millis[3], Piotr Witkowski[3], Vipul Periwal[4], Manami Hara[5]\*, Junghyo Jo[1,6]\***

1 Asia Pacific Center for Theoretical Physics, Pohang, Korea, 2 Meiji University International Institute for Bio-Resource Research, Kanagawa, Japan, 3 Department of Surgery, The University of Chicago, Chicago, IL, United States of America, 4 Laboratory of Biological Modeling, NIDDK, NIH, Bethesda, MD, United States of America, 5 Department of Medicine, The University of Chicago, Chicago, IL, United States of America, 6 Department of Physics, POSTECH, Pohang, Korea

## Abstract

Morphogenesis, spontaneous formation of organism structure, is essential for life. In the pancreas, endocrine $\alpha$, $\beta$, and $\delta$ cells are clustered to form islets of Langerhans, the critical micro-organ for glucose homeostasis. The spatial organization of endocrine cells in islets looks different between species. Based on the three-dimensional positions of individual cells in islets, we computationally inferred the relative attractions between cell types, and found that the attractions between homotypic cells were slightly, but significantly, stronger than the attractions between heterotypic cells commonly in mouse, pig, and human islets. The difference between $\alpha - \beta$ cell attraction and $\beta - \beta$ cell attraction was minimal in human islets, maximizing the plasticity of islet structures. Our result suggests that although the cellular composition and attractions of pancreatic endocrine cells are quantitatively different between species, the physical mechanism of islet morphogenesis may be evolutionarily conserved.

## Introduction

Multi-cellular organisms require communications between neighboring cells, and have developed special architectures for optimizing such cellular communications. A fundamental question in life is how organisms spontaneously form their functional structures. Interestingly, a few simple rules can be sufficient to form complex organs such as the lung [1]. As a microscopic explanation of morphogenesis, Steinberg introduced the *differential adhesion hypothesis* that differences in adhesiveness between cell types are partially responsible for the development and maintenance of organ structures [2,3].

Pancreatic islets of Langerhans are the critical micro-organs responsible for glucose homeostasis. Each islet consists mainly of $\alpha$, $\beta$, and $\delta$ cells. Glucagon and insulin are the reciprocal hormones for increasing and decreasing blood glucose levels, secreted by $\alpha$ and $\beta$ cells, respectively. The role of $\delta$ cells in glucose homeostasis is still mysterious. In addition, it has long been reported that endocrine cells interact with each other [4]. Considering the specific symmetries of interactions between $\alpha$, $\beta$, and $\delta$ cells, their spatial organization must have functional significance. Rodent islets have a shell-core structure where $\beta$ cells are located in the islet core, while non-$\beta$ cells are located on the islet periphery. However, there are contradictory reports regarding the structure of human islets [5]. Some observations suggest more or less random structures of cells [6,7], while others have found some

order in structures, and described human islets as assemblages of $\beta$-cell-core subunits [8] or lobules [9], cloverleaf patterns [5], ribbon-like structures [10], and folded trilaminar plate [11].

Dissociated islet cells spontaneously aggregate and form islet-like structures, *pseudo-islets*, in rat, pig, and human pancreatic cultures [12–15]. Different adhesion molecules have been proposed as a cause of the pseudo-islet formation expressed on rodent $\alpha$ and $\beta$ cells [16–20]. However, the relative adhesion strengths of such cells in native islets has not been directly measured. On one hand, this technical limitation leaves open the interesting question of whether different species have different rules for islet organization. On the other hand, current imaging methods allow to observe islet structures with high resolution. In this study, we computationally infer the organization rule from three-dimensional islet structures. In particular, we compare mouse, pig, and human islets, and find a conserved organization rule behind different islet structures.

## Results

### Cellular distributions in pancreatic islets

Two-dimensional cross sections of pancreatic islets have been widely used to study islet structures. Here, however, we used a confocal microscope to examine three-dimensional islet structures, as previously used [6,21]. To precisely analyze islet structures, we obtained three-dimensional positions of every endocrine cell in

individual islets. We used stained nuclei to determine the center positions of cells, and immunostaining to determine cell types. Figure 1 showed the spatial cellular organizations of pancreatic islets in different species. First, we observed two major cell types of $\alpha$ and $\beta$ cells in mouse (Fig. 1*A*), pig (Fig. 1*B*), and human islets (Fig. 1*C*). Mouse islets showed the typical shell-core structure in which $\beta$ cells are located in the core, while $\alpha$ cells are located on the periphery. In pig and human islets, however, $\alpha$ cells are located not only on the periphery but also distributed inside islets.

We then quantified the fraction of $\beta$ cells depending on islet size in the three species (Fig. 2). Mouse islets consisted of 90% $\beta$ cells independent of islet size. Human islets had a smaller $\beta$-cell fraction, $P_\beta$. In particular, larger human islets had less abundant $\beta$ cells depending on size. This finding in three-dimensional islets is consistent with previous reports based on pancreatic sections [11,22,23]. Interestingly, pig islets ($P_\beta = 0.87 - 0.91$) showed an intermediate characteristic between mouse ($0.91 - 0.94$) and

human islets ($0.62 - 0.78$). We also examined cell-to-cell contacts (See Materials and Methods), and quantified their ratios, $P_{\alpha\alpha}$, $P_{\beta\beta}$, and $P_{\alpha\beta}$ for $\alpha - \alpha$, $\beta - \beta$, and $\alpha - \beta$ contacts, respectively (Fig. 3). The higher $\beta$-cell fraction in mouse islets resulted in more prevalent $\beta - \beta$ contacts ($P_{\beta\beta} = 0.89 - 0.91$), compared with pig ($0.78 - 0.85$) and human islets ($0.46 - 0.64$), but less prevalent $\alpha - \alpha$ and $\alpha - \beta$ contacts.

Given fractions of $\alpha$ and $\beta$ cells, we could simulate cell-to-cell contact probabilities in random cell aggregates. The probability that two sites are occupied randomly by $\alpha$ cells is $P_{\alpha\alpha} = P_\alpha^2$, and the one for $\beta$ cells is $P_{\beta\beta} = P_\beta^2$. In addition, the probability that two sites are occupied randomly by $\alpha$ and $\beta$, or vice versa, is $P_{\alpha\beta} = P_\alpha P_\beta + P_\beta P_\alpha = 2P_\alpha P_\beta$. Regardless of species, Fig. 3 shows that frequencies of homotypic contacts are significantly higher than the probabilities in random aggregates ($P_{\alpha\alpha} > P_\alpha^2$ and $P_{\beta\beta} > P_\beta^2$). On the other hand, islet structures showed smaller frequencies of heterotypic contacts, compared with random ($P_{\alpha\beta} < 2P_\alpha P_\beta$). These results clearly demonstrated that islet structures are not random cell aggregates. This conclusion looks trivial for the shell-core structure of mouse islets (Fig. 1*A*). However, this suggested that pig and human islets also had some order in their cellular organization.

## Self-organization rule for pancreatic islets

Since islets are not random cell aggregates, we investigated rules governing islet structure. Prevalent contacts of homotypic cells could have resulted from (i) replication of neighboring cells and/or (ii) stronger attraction between homotypic cells. Islet organogenesis occurs in the milieu of developmental processes including cell differentiation, migration, aggregation, replication, and death [24,25]. Nevertheless, when islet cells are dissociated, they can spontaneously form pseudo-islets resembling native islets [12–15]. This pseudo-islet formation implies that sequences of complicated developmental processes, particularly cell replication, may not be critical for the formation of equilibrium islet structures. Therefore, as proposed [2,3,26], we investigated if the differential adhesion hypothesis could provide a simple rule governing for islet structures. Depending on the relative adhesiveness between cell types, islets could have various equilibrium structures (Fig. 4). When homotypic attractions are stronger than heterotypic attractions, islets have a sorting phase with two homogeneous cell
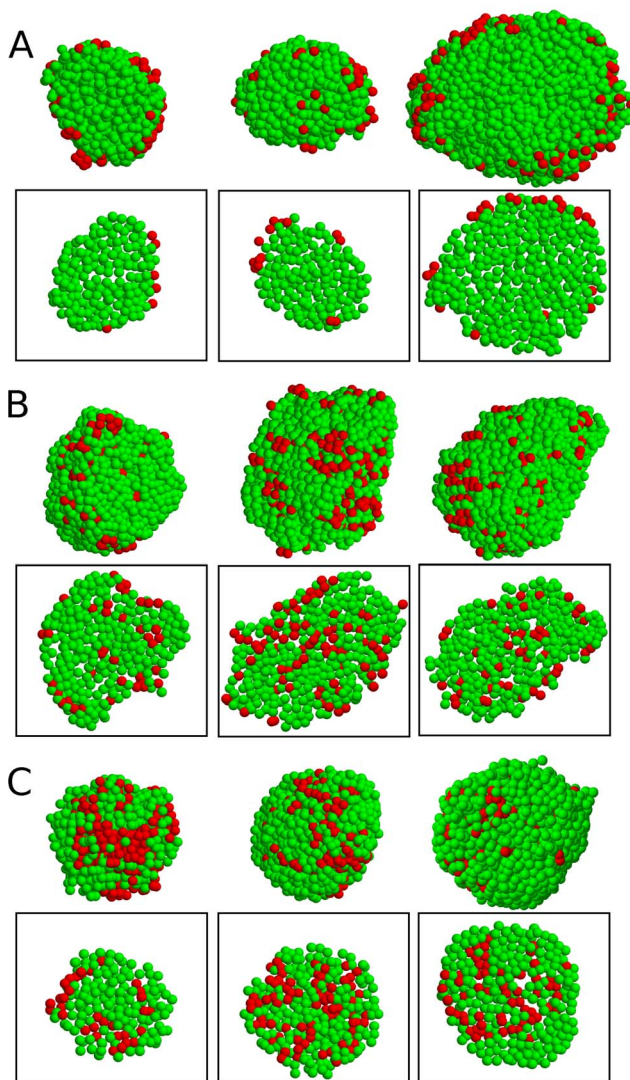


**Figure 1. Cellular organization of pancreatic islets.** Three-dimensional spatial distribution of $\alpha$ cells (red) and $\beta$ cells (green) is shown in (*A*) mouse, (*B*) pig, and (*C*) human islets. To show internal islet structures clearly, their corresponding two-dimensional sections are also shown in boxes.
doi:10.1371/journal.pone.0110384.g001
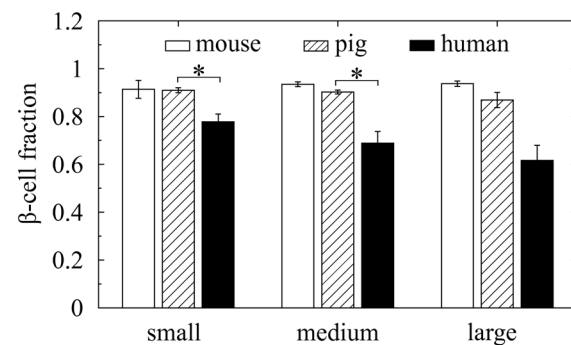


**Figure 2. Cellular compositions in mouse, pig, and human islets.** Fractions of $\beta$ cells, depending on islets size, are calculated in mouse (empty bar), pig (hatched), and human (black solid) islets. Islet size is represented by the total number of cells in islets, and categorized as small (<1000 cells), medium (1000–2000), and large (>2000) islets. Mean $\pm$ SEM (n = 30). $^*P < 0.005$.
doi:10.1371/journal.pone.0110384.g002

**Figure 3. Cell-to-cell contact ratios in mouse, pig, and human islets.** Based on the contacts between neighboring cells, ratios of $\alpha-\alpha$, $\beta-\beta$, and $\alpha-\beta$ contacts ($P_{\alpha\alpha}$, $P_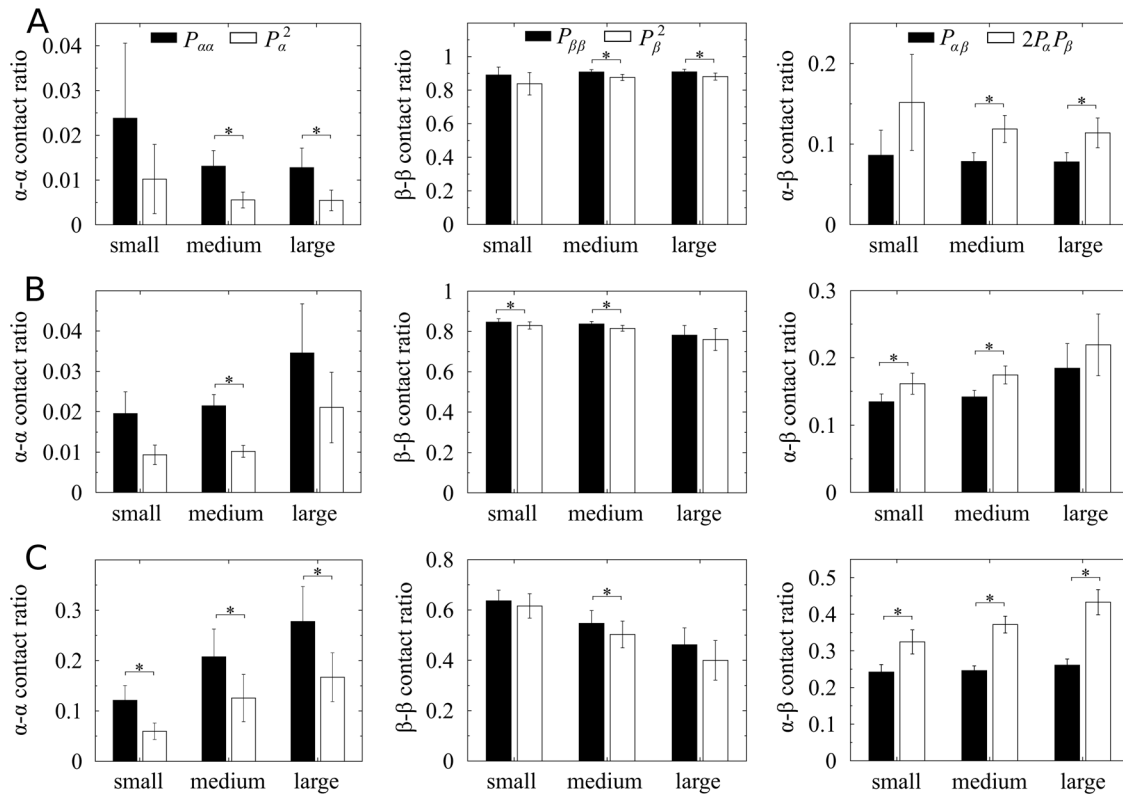{\beta\beta}$, and $P_{\alpha\beta}$), depending on islet size, are calculated in (A) mouse, (B) pig, and (C) human islets. Islet size is represented by the total number of cells in islets, and categorized as small ($<$1000 cells), medium (1000–2000), and large ($>$2000) islets. Given fractions of $\alpha$ and $\beta$ cells ($P_\alpha$ and $P_\beta$), the $\alpha-\alpha$, $\beta-\beta$, and $\alpha-\beta$ contact probabilities in random cell organization are theoretically $P_\alpha^2$, $P_\beta^2$, and $2P_\alpha P_\beta$, respectively. The random organization (empty bar) is compared with the organization of native islets (black solid). Mean $\pm$ SEM. *$P<0.005$.
doi:10.1371/journal.pone.0110384.g003

clusters. As heterotypic attraction becomes stronger, the two cell types start to mix [27].

We specify the relative strengths of adhesiveness or attraction between cell types as $J_{\alpha\alpha}$, $J_{\beta\beta}$, and $J_{\alpha\beta}$ for $\alpha-\alpha$, $\beta-\beta$, and $\alpha-\beta$ contacts, respectively. A stronger attraction between neighboring cells implies that it requires a larger amount of energy to dissociate them. Therefore, the total cell-to-cell contact energy, *self-energy*, in an islet is a sum over every contact

$$E = -J_{\alpha\alpha}N_{\alpha\alpha} - J_{\beta\beta}N_{\beta\beta} - J_{\alpha\beta}N_{\alpha\beta}, \tag{1}$$

where the islet has total $N_{\alpha\alpha}$, $N_{\beta\beta}$, and $N_{\alpha\beta}$ contacts of $\alpha-\alpha$, $\beta-\beta$, and $\alpha-\beta$, respectively. The negative sign in Eq. (1) represents that external energy is needed (not extracted) to dissociate cell-to-cell contacts. Given numbers of $\alpha$ and $\beta$ cells, the islet self-energy can have various values depending on spatial organization of cells. Our conjecture is that islets have an equilibrium structure that



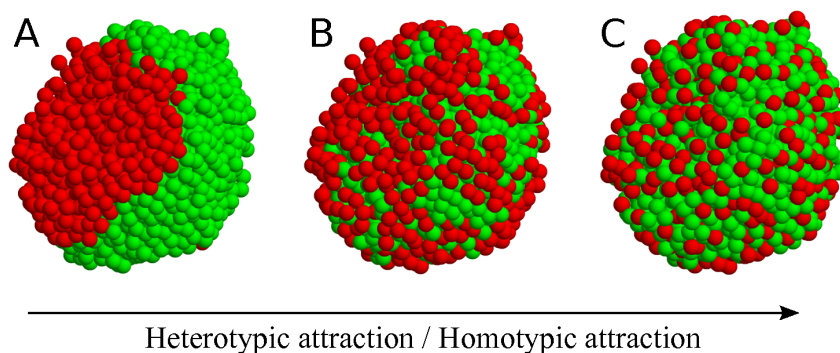Heterotypic attraction / Homotypic attraction

**Figure 4. Schematic diagram of structural dependence on relative attractions between cell types.** A sorting structure of two cell types is changed to mixing structures, as heterotypic attraction increased compared with homotypic attractions: (A) complete sorting, (B) shell-core sorting, and (C) mixing structures.
doi:10.1371/journal.pone.0110384.g004

minimizes their self-energy. When homotypic attractions are stronger, $\alpha - \alpha$ and $\beta - \beta$ contacts are preferred. On the other hand, when heterotypic attraction is stronger, $\alpha - \beta$ contacts are preferred.

Here our problem is not to obtain equilibrium structures given cellular attractions. It is currently not possible to measure the strengths of cellular attractions inside islets. However, we could obtain cell-to-cell contact information from three-dimensional islet imaging. Thus we addressed this inverse problem to infer the strengths of cellular attractions from cell-to-cell contact information. Using Bayesian inference (See Materials and Methods), we inferred the likelihood strengths of cellular attractions that explain observed islet structures. Figure 5 showed the inferred attractions, $J_{\beta\beta}$ and $J_{\alpha\beta}$, relative to the reference attraction $J_{\alpha\alpha} = 1$, from mouse, pig, and human islets. The relative attractions were not dependent on islet size for all species (Fig. S1). Their averages and standard deviations are summarized in Table 1. The relative attractions were not dramatically different between each other, regardless of species. The homotypic attractions, $J_{\alpha\alpha}$ and $J_{\beta\beta}$, were slightly, but significantly, larger than the heterotypic attraction, $J_{\alpha\beta}$, for all species considered. This general conclusion is consistent with the cellular organization, $P_{\alpha\alpha} > P_\alpha^2$, $P_{\beta\beta} > P_\beta^2$, and $P_{\alpha\beta} < 2 P_\alpha P_\beta$. A random organization can be obtained with equal cellular attractions, i.e., $J_{\alpha\alpha} = J_{\beta\beta} = J_{\alpha\beta}$. It is thus understandable that islets have $J_{\alpha\beta} < J_{\alpha\alpha}$ and $J_{\beta\beta}$. However, the Bayesian inference quantified the dependence of relative cellular attractions on species: $J_{\alpha\beta}/J_{\beta\beta}$ for mouse islets (0.91) is lowest, while human islets (0.98 and 0.99 for two different pancreata) show the largest ratio. Pig islets showed a similar ratio (0.97) to human islets.

Here, an intriguing question is whether the small differences in cellular attractions can explain the structural difference between mouse and human islets. In general, binary mixture systems of finite size can generate sorting and mixing phases depending on mixture fraction and relative adhesion strengths [27]. To answer the question, we considered two theoretical lattices representing
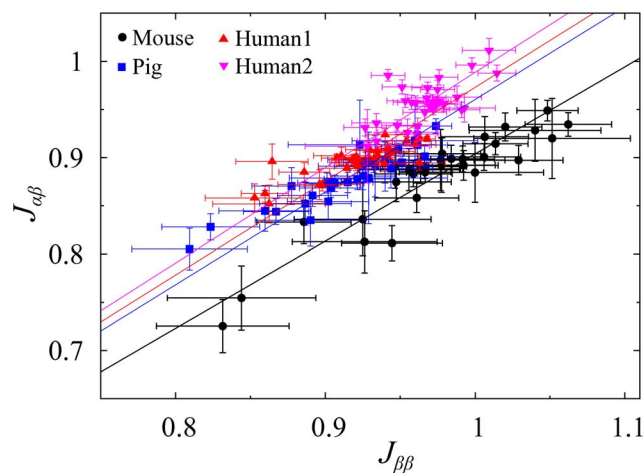
islet structures: cubic (Fig. 6A) and hexagonal close packed (HCP) lattices (Fig. 6B), in which $\alpha$ and $\beta$ cells are distributed with various $\beta$-cell fractions $P_\beta$ and relative attraction strengths $J_{\alpha\beta}/J_{\beta\beta}$. Then we computed cell-to-cell contact numbers and their fluctuations, and obtained the phase diagrams for the cubic lattice (Fig. 7A) and the HCP lattice (Fig. 7B). Human and pig islets were classified to have the partial mixing structure for both cubic and HCP lattices. However, mouse islets were classified to have the partial mixing structure for the cubic lattice, but to have the shell-core sorting structure for the HCP lattice. The native islet structure could be approximated better as the HCP lattice than the cubic lattice, because its mean number of neighboring cells ($8.6 \pm 0.3$ for mouse, $8.5 \pm 0.3$ for pig, $8.4 \pm 0.3$ for Human1, and $8.3 \pm 0.6$ for Human2 islets) was closer to the HCP lattice (10.6) than the cubic lattice (5.4). Therefore, we concluded that the higher $\beta$-cell fraction $P_\beta$ and the slightly weaker heterotypic attraction $J_{\alpha\beta}/J_{\beta\beta}$ of mouse islets could be sufficient to generate the shell-core sorting structure, distinct from the partial mixing structure of human and pig islets.

## Spatial organization of δ cells

In addition to $\alpha$ and $\beta$ cells, islets contain a minor population of somatostatin-secreting $\delta$ cells. We further examined human islet structures including $\delta$ cells (Fig. 8). Similarly to previous analysis, we inferred cellular attractions, relative to $\alpha - \alpha$ attraction ($J_{\alpha\alpha} = 1$), not only $J_{\beta\beta}$ and $J_{\alpha\beta}$, but also $J_{\delta\delta}$, $J_{\alpha\delta}$, and $J_{\beta\delta}$ (Table 2). The result could be summarized as $J_{\alpha\alpha} \approx J_{\beta\beta} \approx J_{\delta\delta} > J_{\alpha\beta} \approx J_{\alpha\delta} \approx J_{\beta\delta}$. In general, homotypic attractions were slightly stronger than heterotypic attractions.

To validate our previous analysis with islets in which $\delta$ cells are unseen, we inferred $J_{\beta\beta}$ and $J_{\alpha\beta}$ from islets in which $\delta$ cells are seen, but ignored as empty sites. Their inferred values were not different regardless of the presence and absence of $\delta$ cells (Table 2).

## Discussion

We observed spatial distributions of endocrine cells in three-dimensional islets, and characterized their distributions in mouse, pig, and human islets. Islets from different species showed different cellular compositions and structures. An intriguing question was whether the structural difference originates from the different cellular composition or different organization rules, or both. Based on our computational inference from the high-resolution islet structures, we found that the adhesions between homotypic cells were slightly, but significantly, stronger than the ones between heterotypic cells commonly in the three species. Furthermore, the binary mixture simulation on the HCP lattice demonstrated that the small difference of relative adhesions and the more abundant $\beta$ cells could generate the shell-core structure of mouse islets, which was different from the partial mixing structure of pig and human islets. Therefore, the conserved rule could explain the different islet organizations of the three species.

We considered islet organogenesis as an equilibrium process assuming that given numbers of cells can switch their positions and minimize their total contact energy, the islet self-energy. One might consider it as a non-equilibrium process where the sequential events of cell differentiation and replication elaborately construct the specific structures of islets during development. However, sequential development is limited to explain the following two observations. First, cell replication could explain the preferential neighboring of homotypic cells, but it could not explain the regional segregation of $\alpha$ cells and $\beta$ cells in mouse islets without extra processes such as cell polarization, migration,



**Figure 5. Cellular attractions in mouse, pig, and human islets.** Relative attractions between cell types and their uncertainties are inferred from three-dimensional islet structures. Symbols represent individual islets: mouse (black circle), pig (blue square), and human islets (red triangle and pink inverse triangle). Each species has n = 30 islets. In particular, two sets of n = 30 islets are provided from two human (Human1 and Human2) subjects. The relationship between $J_{\alpha\beta}$ and $J_{\beta\beta}$ is fitted with linear functions, $y = ax$, represented by solid lines with colors corresponding to each species. Note that the attraction between $\alpha$ cells is defined as a reference attraction, $J_{\alpha\alpha} = 1$.
doi:10.1371/journal.pone.0110384.g005

**Table 1.** Cellular attractions in mouse, pig, and human islets.

| Species | n | $J_{\beta\beta}$ | $J_{\alpha\beta}$ | $J_{\alpha\beta}/J_{\beta\beta}$ |
|---|---|---|---|---|
| Mouse | 30 | $0.97\pm0.05$ | $0.88\pm0.05^{a}$ | $0.91\pm0.02$ |
| Pig | 30 | $0.91\pm0.04$ | $0.88\pm0.03^{a}$ | $0.97\pm0.02^{b}$ |
| Human1 | 30 | $0.92\pm0.03$ | $0.90\pm0.02^{a}$ | $0.98\pm0.02$ |
| Human2 | 30 | $0.97\pm0.02$ | $0.96\pm0.02^{a}$ | $0.99\pm0.02$ |

Relative attractions between cell types are inferred from three-dimensional islet structures, mean $\pm$ SD (n = 30 islets). Note that the attraction between $\alpha$ cells is defined as a reference attraction, $J_{\alpha\alpha}=1$.
[a]Paired Student's t-test concludes $J_{\beta\beta}>J_{\alpha\beta}$ with $P<0.005$.
[b]Unpaired Student's t-test concludes that mouse and pig islets have different $J_{\alpha\beta}/J_{\beta\beta}$ with $P<0.005$.
doi:10.1371/journal.pone.0110384.t001

and death. In contrast, the equilibrium process, based on the differential adhesion hypothesis, may provide a simpler explanation for the regional segregation problem. Second, when endocrine cells are dissociated from mature islets, they can re-aggregate and form pseudo-islets resembling the native islets [12–15]. The pseudo-islet formation gives direct evidence suggesting that the sequence of developmental events might not be critical for the determination of islet structures. Assuming that cellular motility is sufficiently large, the detailed history of cell additions through differentiation and replication may not significantly affect the equilibrium islet structures.

Here we proposed a *dynamic structure* of islets, balancing cell motility and adhesion, instead of a static structure where cellular positions were frozen. Lymphocyte homing is an extreme example of a dynamic structure because highly mobile immune cells can organize lymphoid organs such as germinal centers and Peyer's patches through chemotaxis and adhesion [28,29]. In this study, we quantified the cellular attraction $J_{xy}$ as a required energy to dissociate the contact of $x$ and $y$ cells, and represented the cell motility $T$ as a kind of fluctuation energy to help the cellular contacts dissociate. As the cell motility $T$ increased, cells could break their contacts to neighboring cells more frequently and move more actively. Our analysis showed that the the relative attractions between cell types were not dramatically different in

pancreatic islets. Quantitatively, the energy gap between the relative cellular attractions did not exceed the fluctuation energy for cell motility to dissociate the cellular contacts, $J_{\beta\beta}-J_{\alpha\beta}<T$.



**Figure 7. Phase diagrams of binary mixtures.** Binary mixtures have complete sorting (white region), shell-core sorting (cyan region), partial mixing (yellow region), and complete sorting (gray region) structures depending on mixture fraction and relative adhesion strengths. Plotted are phase diagrams for (A) cubic and (B) hexagonal close packed lattices with 1357 cells. Symbols represent the observed $\beta$-cell fraction $P_\beta$ and the inferred relative attraction $J_{\alpha\beta}/J_{\beta\beta}$ of mouse islets (black circle), pig (blue square), and human islets (red triangle and pink inverse triangle). Note that the homotypic attractions have a reference attraction, $J_{\alpha\alpha}=J_{\beta\beta}=1$. Each species has n = 30 islets. Mean $\pm$ SD.
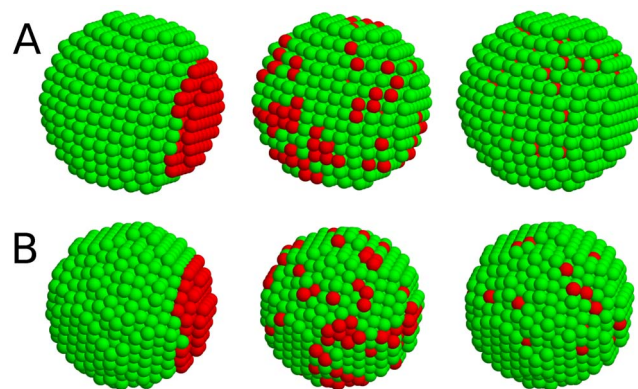doi:10.1371/journal.pone.0110384.g007



**Figure 6. Distinct structures of binary mixtures.** Complete sorting, shell-core sorting, and partial mixing structures are plotted for (A) cubic and (B) hexagonal close packed lattices. Here each lattice consists of 1357 cells with 10% $\alpha$ cells (red) and 90% $\beta$ cells (green). The relative attractions are chosen to have the specific structures: $J_{\alpha\beta}=0.7$ (left), 0.85 (middle), and 1.1 (right) for (A) the cubic lattice; and $J_{\alpha\beta}=0.7$ (left), 0.93 (middle), and 1.1 (right) for (B) the hexagonal close packed lattice. Note that the homotypic attractions are fixed as a reference, $J_{\alpha\alpha}=J_{\beta\beta}=1$, and the thermal fluctuation energy is $T=0.2$.
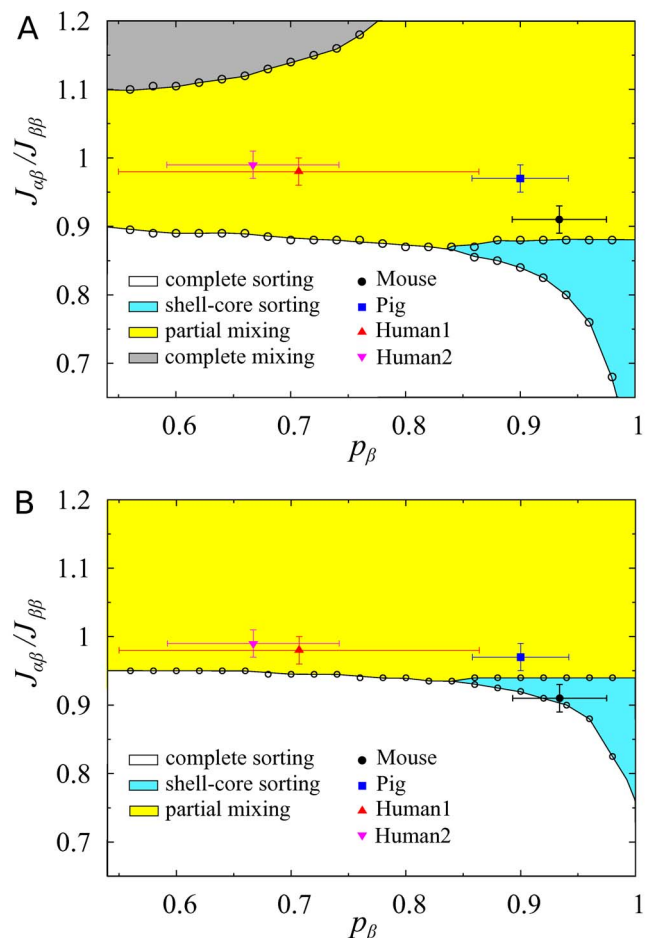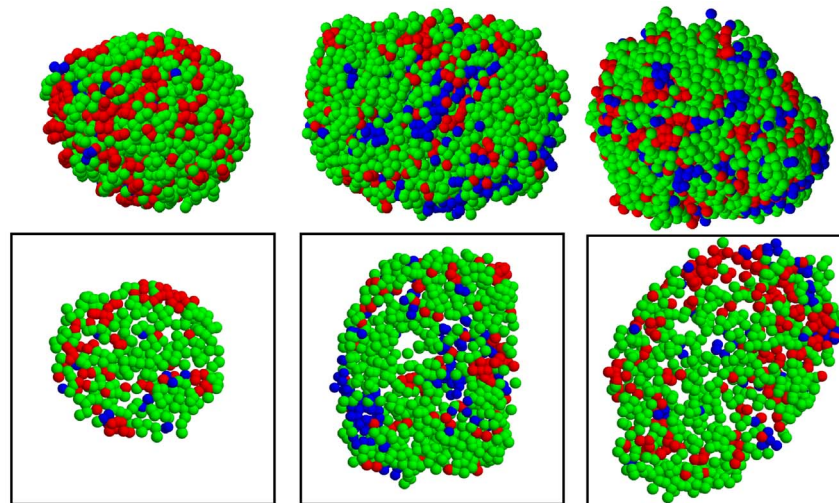doi:10.1371/journal.pone.0110384.g006

**Figure 8. Cellular organization of human pancreatic islets.** Three-dimensional spatial distribution of $\alpha$ cells (red), $\beta$ cells (green), and $\delta$ cells (blue) in human islets is shown. To show internal islet structures clearly, their corresponding two-dimensional sections are also shown in boxes. Note that islets are isolated from the Human3 subject for this plot.
doi:10.1371/journal.pone.0110384.g008

Thus islet structures become rather different from random cell organization to have a few more contacts between homotypic cells. The fine balancing of cell adhesion and motility may allow islets to have flexible structures. In particular, human islets had the minimal energy gap, $J_{\beta\beta} - J_{\alpha\beta}$, which could maximize the structural plasticity of islets. Note that this might explain the prima facie contradictory observations of human islet structure, random versus ordered structures [5]. The morphogenetic plasticity of islets has been observed [30], and proposed to have a functional implication under altered physiological conditions [31]. The islet morphology of diabetic (*db/db*) and pregnant mice shows the partial mixing structure of human islets instead of the typical shell-core sorting structure of rodent islets [31].

The differential adhesiveness between islet cells may originate from the differential expression of adhesion molecules on their cell membranes. Indeed the differential expression of neural cell adhesion molecule (NCAM) between $\beta$ and non-$\beta$ cells has been observed in rodent islets [17]. Furthermore, to quantify the cellular adhesiveness, the cohesivity of spherical aggregates of islet cell lines has been measured [20]. Nevertheless, it still remains to examine the expression levels of different adhesion molecules on $\alpha$, $\beta$, and $\delta$ cells in different species, and find the correlation between their relative expressions and the physical attractions between cell types. In addition to the experimental demonstration of the conserved rule for the islet organization, its physiological reason remains to investigate. The coupling between $\beta$ cells through gap junctions has been emphasized to pronounce insulin secretion [32]. Furthermore, the functional roles of paracrine interactions between $\alpha$, $\beta$, and $\delta$ cells have been recently investigated [33,34]. The slight preference of $\beta - \beta$ contacts to $\beta - \alpha$ and $\beta - \delta$ contacts may allow islets to have both advantages of $\beta$-cell coupling and paracrine interactions.

## Materials and Methods

### Ethics Statement

Mouse studies were approved by the Institutional Animal Care and Use Committee of the University of Chicago. Pig studies were approved by the Institutional Animal Care and Use Committee of Meiji University. The use of human tissues in the study was approved by the Institutional Review Board at the University of Chicago.

### Mouse, pig, and human islets

Mouse islets were isolated from a 3-mo old male mouse on CD-1 background. Pig islets were isolated from a 4.5-mo old female pig (a crossbred of Large white/Landrace and Duroc). Human pancreata (Human1: 60-year-old male and BMI 39.5; Human2: 40-year-old female and BMI 53; Human3: 51-year-old female and BMI 29.3) were generously provided by the Gift of Hope Organ and Tissue Donor Network in Chicago. Written informed consent from a donor or the next of kin was obtained for use of a sample in research. Specimens were collected within 12 hours of cold ischemia.

### Immunohistochemistry

Isolated islets were stained with the following primary antibodies (all 1:500): polyclonal guinea pig anti-porcine insulin (DAKO, Carpinteria, CA), mouse monoclonal anti-human glucagon (Sigma-Aldrich, St. Louis, MO), polyclonal goat anti-somatostatin (Santa Cruz, Santa Cruz, CA), and DAPI (Invitrogen, Carlsbad, CA). The primary antibodies were detected using a combination of DyLight 488, 549, and 649-conjugated secondary antibodies (1:200, Jackson ImmunoResearch Laboratory, West Grove, PA).

### Confocal microscopy

Microscopic images were taken with an Olympus IX8 DSU spinning disk confocal microscope (Melville, NY). To obtain coordinates of each islet cell, we manually scanned XYZ directions of a given islet, identified DAPI-stained nuclei, and determined corresponding cell types via endocrine hormone staining (i.e., insulin, glucagon, or somatostatin).

### Determination of cellular contacts

Neighboring contacts between cells were determined based on intercellular distance and angle. Note that the neighbor determination is not trivial in soft tissues unlike regular lattices. For each cell, we defined a set of cells located within a threshold distance $D$ as its neighbors. Then, to discriminate some neighbors which are

**Table 2.** Cellular compositions and attractions in human islets.

| No. | Size | $P_\alpha$ | $P_\beta$ | $P_\delta$ | $J_{\beta\beta}$ | $J_{\alpha\beta}$ | $J_{\delta\delta}$ | $J_{\alpha\delta}$ | $J_{\beta\delta}$ |
|---|---|---|---|---|---|---|---|---|---|
| 1 | 588 | 0.25 | 0.54 | 0.21 | 0.97±0.02(0.96) | 0.92±0.01(0.91) | 1.03±0.02 | 0.93±0.02 | 0.90±0.02 |
| 2 | 2096 | 0.31 | 0.56 | 0.13 | 1.00±0.01(1.00) | 0.94±0.01(0.93) | 1.01±0.02 | 0.90±0.01 | 0.90±0.02 |
| 3 | 2264 | 0.19 | 0.65 | 0.16 | 0.96±0.01(0.97) | 0.91±0.01(0.91) | 1.00±0.02 | 0.90±0.01 | 0.89±0.02 |
| 4 | 2858 | 0.29 | 0.48 | 0.23 | 0.97±0.01(0.99) | 0.92±0.004(0.93) | 0.99±0.01 | 0.93±0.01 | 0.89±0.01 |
| 5 | 3253 | 0.34 | 0.47 | 0.19 | 0.98±0.01(0.99) | 0.93±0.005(0.93) | 1.00±0.01 | 0.91±0.01 | 0.89±0.01 |
| 6 | 3544 | 0.27 | 0.63 | 0.10 | 0.97±0.01(0.97) | 0.92±0.005(0.92) | 1.03±0.03 | 0.93±0.02 | 0.91±0.02 |
| Av. | 2434 | 0.28 | 0.55 | 0.17 | 0.98±0.01(0.98) | 0.92±0.01(0.92) | 1.01±0.02 | 0.92±0.02 | 0.90±0.01 |

Fractions of $\alpha$, $\beta$, and $\delta$ cells in six human islets, isolated from the Human3 subject, are calculated. Islet size is represented by the total number of cells in islets. Relative attractions between cell types are inferred from three-dimensional islet structures, mean ± SD. Note that the attraction between $\alpha$ cells is defined as a reference attraction, $J_{\alpha\alpha}=1$. The values $J_{\beta\beta}$ and $J_{\alpha\beta}$ in parentheses are inferred from the three-dimensional islet structures ignoring $\delta$ cells as empty sites.

doi:10.1371/journal.pone.0110384.t002

located close but not contacting, we measured intercellular angles between the vectors from a given vertex of each cell to its neighbors (Fig. S2). The neighbors forming narrow intercellular angles could be second-nearest neighbors. Therefore we removed those neighbors forming angles below a threshold angle $\Theta$ from the neighbor set of each cell. The double criteria could exclude potential errors for determining neighboring cells in large islets perhaps slightly flattened due to gravity. In practice, the mean distance between nearest nuclei can be approximated as cell diameter $d$. In a cubic lattice (having 6 nearest neighbors) and a hexagonal close packed lattice (12 nearest neighbors), the distances to second-nearest neighbors are $\sqrt{2}d$ and $\sqrt{3}d$, respectively. In addition, their intercellular angles between nearest neighbors are $\pi/2$ and $\pi/3$. These values could guide upper limits for $D$ and $\Theta$. We optimized these thresholds $D$ and $\Theta$ to obtain a reasonable neighboring number distribution (8 to 9 neighbors on average, 12 neighbors at most, and 1 neighbor at least). We have checked that our results were not sensitive to the thresholds.

## Model equilibration

The islet self-energy based on cellular attractions is

$$E=-\sum_{i}\sum_{j\in\Lambda_i}J_{\sigma_i\sigma_j}, \tag{2}$$

where $\sigma_i=\{\alpha,\beta,\delta\}$ represents the cell type at the $i$th site, $J_{\sigma_i\sigma_j}$ denotes the relative attractions between $\sigma_i$ and $\sigma_j$, and $\Lambda_i$ represents nearest neighbors of the $i$th site. Given cellular coordinates in an islet structure, we minimized its self-energy by exchanging positions of cells. Monte-Carlo simulation was used for the equilibration of islet structures for given cellular attractions, $J_{xy}$ with $x,y=\{\alpha,\beta,\delta\}$ [27]. We started from measured islet structures where cell positions and types were specified. Briefly, we (i) randomly distributed given numbers of $\alpha$, $\beta$, and $\delta$ cells at the given cell coordinates in the islet; (ii) randomly chose two cells to swap, and calculated islet self-energies of $E$ and $E'$ before and after exchanging their positions; (iii) accepted the exchange with the probability, $\min\{1,\exp(-\Delta E/T)\}$, where $\Delta E=E'-E$ and $T$ denotes thermal fluctuation, following the Metropolis algorithm [35]; and (iv) repeated these procedures in several million Monte-Carlo steps per cell to obtain an equilibrium islet structure for given cellular attractions. After equilibration, we recorded cell-to-cell contact numbers $N_{xy}$ during another million Monte-Carlo steps, and calculated their mean $\bar{N}_{xy}$ and variance $\delta N_{xy}^2$. Note that this procedure is basically the same for considering the islets having only $\alpha$ and $\beta$ cells by ignoring $\delta$ cells.

## Bayesian inference of cellular attractions

Our aim is not to obtain an equilibrium structure given cellular attraction energies, but to infer these energies given an observed structure. The basic idea is to search enumerated sets of cellular attractions, $\mathbf{J}=\{J_{xy}\}$ with $x,y=\{\alpha,\beta,\delta\}$, and find the likelihood sets that can explain the observed structure (Fig. S3). Summarizing, we (i) generated a random set of $\mathbf{J}$; (ii) obtained an equilibrium structure given $\mathbf{J}$; (iii) calculated the mean $\bar{N}_{xy}$ and the variance $\delta N_{xy}^2$ of cell-to-cell contact numbers between $x$ and $y$ cell types for the equilibrium structure, as explained in the previous section; (iv) compared the equilibrium structure with the observed structure in terms of cell-to-cell contact numbers by quantifying their mismatches:

$$M(\mathbf{J}) = \sum_{x,y} \frac{(\bar{N}_{xy} - N_{xy})^2}{2\delta N_{xy}^2} \qquad (3)$$

where $N_{xy}$ are the cell-to-cell contact numbers in the observed islet structures; and (v) repeated these procedures with a new set of $\mathbf{J}$ for several tens of thousands of trials. The likelihood of $\mathbf{J}$ for the observed cell-to-cell contact numbers, $\mathbf{N} = \{N_{xy}\}$, becomes

$$P(\mathbf{J}|\mathbf{N}) = \frac{e^{-M(\mathbf{J})}}{\sum e^{-M(\mathbf{J})}} \qquad (4)$$

thanks to the maximum entropy principle [36]. Here the summation represents all the trials of $\mathbf{J}$ sets. Then, given all the trials or ensemble of $\mathbf{J}$, we finally could infer the mean $\bar{J}_{xy}$ and the variance $\delta J_{xy}$ of cellular attractions for the observed islet structure:

$$\bar{J}_{xy} = \sum J_{xy} P(\mathbf{J}|\mathbf{N}), \qquad (5)$$

$$\delta J_{xy}^2 = \sum J_{xy}^2 P(\mathbf{J}|\mathbf{N}) - \bar{J}_{xy}^2. \qquad (6)$$

In order to optimize the calculation time, we choose $\mathbf{J}$ in a focus zone where the mismatch value $M(\mathbf{J})$ is not so large, instead of generating $\mathbf{J}$ at random. For the simulation, the relative attractions $J_{\alpha\alpha} = 1$ is used as unit of energy, and the fluctuation energy, which is a determinant of cell motility, is chosen large enough to escape local minimum of self-energy landscape for $\mathbf{J}$, but low enough not to exceed cellular attraction energies. In particular, the fluctuation energy should be clearly less than the cellular attraction energies ($T < J_{xy}$). Otherwise, too large motility could detach cells from their aggregates under free boundary conditions. Therefore, we chose a reasonable fluctuation energy $T = 0.2$. However, our conclusion was robust to different fluctuation energies (e.g., $T = 0.5$; Table S1; Fig. S4).

## Phase diagram of binary mixtures

Pancreatic islets could be considered as a binary mixture of $\alpha$ and $\beta$ cells, the two dominant populations. In general, binary mixtures in finite systems have sorting and mixing phases depending on their composition and relative adhesion strengths between cell types. As the ratio of heterotypic attraction to homotypic attraction increases, the binary mixture has four distinct structures: complete sorting, shell-core sorting, partial mixing, and complete mixing phases [27]. We computed cell-to-cell contact numbers and their fluctuations with various $\beta$-cell fractions and relative attraction strengths for $\alpha-\alpha$, $\beta-\beta$, and $\alpha-\beta$ contacts. The contact number fluctuations were peaked at the boundaries between the distinct phases (Fig. S5), representing phase transitions. Based on the fluctuations, we could identify distinct structures of the binary mixture (Fig. 6), and obtained their phase diagram. For the theoretical phase diagram, we used both cubic and HCP lattices. The lattice size was fixed to have 1357 cells for both lattices. Note that the phase diagrams were not sensitive to the lattice size within the range of islet size.

## Supporting Information

**Figure S1 Relative cellular attractions and islet size.** Relative attractions between cell types are inferred from three-dimensional islet structures in (A) mouse, (B) pig, and two human,

(C) Human1 and (D) Human2, subjects. Islet size is represented by the total number of cells in islets. Symbols represent individual islets, and lines represent linear data fits (dotted blue). Here the linear regression analysis rejects the null hypothesis that the relative cellular attractions depend on islet size with high $P$ values for mouse ($P = 0.48$), pig (0.87), Human1 (0.03), and Human2 (0.20). $R$ values in the plots represent the coefficient of determination. Note that the attraction between $\alpha$ cells is defined as a reference attraction, $J_{\alpha\alpha} = 1$. Here thermal fluctuation energy is $T = 0.2$.
(TIF)

**Figure S2 Determination of cellular contacts.** Neighboring cells that contact to a given cell (cyan) are determined by cellular distance $r$ and angle $\theta$. Sometimes second-nearest neighboring cells can be located within a threshold distance $D$ for determining neighbors. In the diagram, nearest-neighboring (red) and second-nearest neighboring (green) cells are defined as neighbors just based on distance ($r < D$). However, once we include them, intercellular angles ($\theta = \angle AOB$) between the neighbors can be smaller than an angle threshold $\Theta$. The angle threshold ($\theta < \Theta$) can be used to further discriminate neighboring cells, close to the given cell (cyan), but not contacting.
(TIF)

**Figure S3 Flow chart for model equilibration and Bayesian inference.** We generate cellular attraction energies, $\mathbf{J} = \{J_{xy}\}$ with $x, y = \{\alpha, \beta, \delta\}$, which are parameters of the differential adhesion model. Then, by using Monte-Carlo simulation, we equilibrate the islet self-energy, $E = -\sum_{x,y} J_{xy} N_{xy}$, given $J_{xy}$, where $N_{xy}$ are the contact numbers between $x$ and $y$ cells. After equilibration, we obtain average numbers of cellular contacts $\bar{N}_{xy}$, and their fluctuations $\delta N_{xy}$. Finally, we compute the mismatch between predicted cellular contact numbers and the measured ones, $N_{xy}$. By repeating this procedure, we can have likelihood distribution of $J_{xy}$, given cellular contacts $\mathbf{N} = \{N_{xy}\}$. This allows to estimate the likelihood $\bar{J}_{xy}$ and its uncertainty $\delta J_{xy}$.
(TIF)

**Figure S4 Cellular attractions at high thermal fluctuations.** Relative attractions between cell types and their uncertainties are inferred from three-dimensional islet structures. Symbols represent individual islets: mouse (black circle), pig (blue square), and human islets (red triangle and pink inverse triangle). Each species has n = 30 islets. In particular, two sets of n = 30 islets are provided from two human (Human1 and Human2) subjects. The relationship between $J_{\alpha\beta}$ and $J_{\beta\beta}$ is fitted with linear functions, $y = ax$, represented by solid lines with colors corresponding to each species. Note that the attraction between $\alpha$ cells is defined as a reference attraction, $J_{\alpha\alpha} = 1$. Here thermal fluctuation energy is $T = 0.5$.
(TIF)

**Figure S5 Cell-to-cell contact number fluctuations.** The binary mixture of $\alpha$ cells (40%) and $\beta$ cells (60%) generates different structures depending on the relative attractions between cell types. For this plot, we fix the homotypic attractions as a reference, $J_{\alpha\alpha} = J_{\beta\beta} = 1$, and vary the heterotypic attraction $J_{\alpha\beta}$. Note that the thermal fluctuation energy is $T = 0.2$. At equilibrium, the contact numbers between cell types have fluctuations, which are peaked at the boundaries between distinct structures. Here we use (A) cubic and (B) hexagonal close packed lattices with 1357 cells.
(TIF)

**Table S1  Cellular attractions at high thermal fluctuations.**
(PDF)

## Author Contributions

Conceived and designed the experiments: DH VP MH JJ. Performed the experiments: HM MN HN JM PW MH. Analyzed the data: DH VP JJ. Contributed reagents/materials/analysis tools: HN JM PW VP MH JJ. Wrote the paper: DH VP MH JJ.

## References

1. Metzger RJ, Klein OD, Martin GR, Krasnow MA (2008) The branching programme of mouse lung development. Nature 453: 745–750.
2. Steinberg MS (1963) Reconstruction of tissues by dissociated cells. Science 141: 401–408.
3. Steinberg MS (2007) Differential adhesion in morphogenesis: a modern view. Curr Opin Genet Dev, 17: 281–286.
4. Kelly C, McClenaghan NH, Flatt PR (2011) Role of islet structure and cellular interactions in the control of insulin secretion. Islets 3: 41–47.
5. Bonner-Weir S, O'Brien T (2008) Islets in type 2 diabetes: in honor of dr. robert c. turner. Diabetes 57: 2899–2904.
6. Brissova M, Fowler MJ, Nicholson WE, Chu A, Hirshberg B, et al. (2005) Assessment of human pancreatic islet architecture and composition by laser scanning confocal microscopy. J Histochem Cytochem 53: 1087–1097.
7. Cabrera O, Berman DM, Kenyon NS, Ricordi C, Berggren PO, et al. (2006) The unique cytoarchitecture of human pancreatic islets has implications for islet cell function. Proc Natl Acad Sci USA 103: 2334–2339.
8. Orci L (1976) The microanatomy of the islets of langerhans. Metabolism 25: 1303–1313.
9. Erlandsen SL, Hegre OD, Parsons JA, McEvoy RC, Elde RP (1976) Pancreatic islet cell hormones distribution of cell types in the islet and evidence for the presence of somatostatin and gastrin within the d cell. J Histochem Cytochem 24: 883–897.
10. Grube D, Deckert I, Speck PT, Wagner HJ (1983) Immunohistochemistry and microanatomy of the islets of langerhans. Biomed Res 4: 25–36.
11. Bosco D, Armanet M, Morel P, Niclauss N, Sgroi A, et al. (2010) Unique arrangement of α- and β-cells in human islets of langerhans. Diabetes 59: 1202–1210.
12. Halban PA, Powers SL, George KL, Bonner-Weir S (1987) Spontaneous reassociation of dispersed adult rat pancreatic islet cells into aggregates with three-dimensional architecture typical of native islets. Diabetes 36: 783–790.
13. Hopcroft DW, Mason DR, Scott RS (1985) Insulin secretion from perifused rat pancreatic pseudoislets. In Vitro Cell Dev Biol 21: 421–427.
14. Britt LD, Stojeba PC, Scharp CR, Greider MH, Scharp DW (1981) Neonatal pig psedu-islets: a product of selective aggregation. Diabetes 30: 580–583.
15. Kuo CY, Herrod HG, Burghen GA (1992) Formation of pseudoislets from human pancreatic cultures. Pancreas 7: 320–325.
16. Halban PA, Powers SL, George KL, Bonner-Weir S (1988) Altered differentiated cell surface properties of transformed (rinm5f) compared with native adult rat pancreatic b cells. Endocrinology 123: 113–119.
17. Rouiller DG, Cirulli V, Halban PA (1990) Differences in aggregation properties and levels of the neural cell adhesion molecule (ncam) between islet cell types. Exp Cell Res 1917: 305–312.
18. Rouiller DG, Cirulli V, Halban PA (1991) Uvomorulin mediates calcium-dependent aggregation of islet cells, whereas calcium-independent cell adhesion molecules distinguish between islet cell types. Dev Biol 148: 233–242.
19. Cirulli V, Baetens D, Rutishauser U, Halban PA, Orci L, et al. (1994) Expression of neural cell adhesion molecule (n-cam) in rat islets and its role in islet cell type segregation. J Cell Sci 107: 1429–1436.
20. Jia D, Dajusta D, Foty RA (2007) Tissue surface tensions guide in vitro self-assembly of rodent pancreatic islet cells. Dev Dyn 236: 2039–2049.
21. Brelje TC, Scharp DW, Sorenson RL (1989) Three-dimensional imaging of intact isolated islets of langerhans with confocal microscopy. Diabetes 38: 808–814.
22. Kim A, Miller K, Jo J, Kilimnik G, Wojcik P, et al. (2009) Islet architecture: a comparative study. Islets 1: 129–136.
23. Kilimnik G, Zhao B, Jo J, Periwal V, Witkowski P, et al. (2011) Altered islet composition and disproportionate loss of large islets in patients with type 2 diabetes. PLoS ONE 6: e27445.
24. Slack JMW (1995) Developmental biology of the pancreas. Development 121: 1569–1580.
25. Edlund H (2002) Pancreatic organogenesis – developmental mechanisms and implications for therapy. Nat Rev Genet 3: 524–532.
26. Gumbiner BM (1996) Cell adhesion: the molecular basis of tissue architecture and morphogenesis. Cell 84: 345–357.
27. Hoang DT, Song J, Jo J (2013) Partial mixing phase of binary cells in finite systems. Phys Rev E 88: 062725.
28. Butcher EC, Picker LJ (1996) Lymphocyte homing and homeostasis. Science 272: 60–66.
29. Mebius RE (2003) Organogenesis of lymphoid tissues. Nat Rev Immunol 3: 292–303.
30. Jamal AM, Lipsett M, Sladek R, Laganière S, Hanley S, et al. (2005) Morphogenetic plasticity of adult human pancreatic islets of langerhans. Cell Death Differ 12: 702–712.
31. Steiner DJ, Kim A, Miller K, Hara M (2010) Pancreatic islet plasticity: interspecies comparison of islet architecture and composition. Islets 2: 135–145.
32. Charollais A, Gjinovci A, Huarte J, Bauquis J, Nadal A, et al. (2000) Junctional communication of pancreatic β cells contributes to the control of insulin secretion and glucose tolerance. J Clin Invest 106: 235–243.
33. Jo J, Choi MY, Koh DS (2009) Beneficial effects of intercellular interactions between pancreatic islet cells in blood glucose regulation. J Theor Biol 257: 312–319.
34. Hong H, Jo J, Sin SJ (2013) Stable and flexible system for glucose homeostasis. Phys Rev E 88: 032711.
35. Metropolis N, Ulam S (1949) The monte carlo method. J Am Statist Assoc 44: 335–341.
36. Sivia DS, Skilling J (2006) Data Anlysis - A Bayesian Tutorial. Oxford University Press.